Available online at www.sciencedirect.com
SCIENCE DIRECT®
Journal of the European Ceramic Society 25 (2005) 535–542
www.elsevier.com/locate/jeurceramsoc

Tensile strength and fiber/matrix interfacial properties of 2D- and 3D-carbon/carbon composites

Hiroshi Hatta [a,*], Ken Goto [a], Shinya Ikegaki [b], Itaru Kawahara [c], Mohamed S. Aly-Hassan [a], Hiroyuki Hamada [b]

[a] *Research Division of Space Structure and Materials, The Institute of Space and Astronautical Science, Japan Aerospace Exploration Agency, 3-1-1 Yoshinodai, Sagamihara, Kanagawa 229-8510, Japan*
[b] *Advanced Fibro-Science, Kyoto Institute of Technology, Matsugasaki Sakyo-ku, Kyoto 606-8585, Japan*
[c] *Graduate School of Engineering, Kogakuin University, 2665-1 Nakano-chou, Hachioji, Tokyo 192-0015, Japan*

Received 28 August 2003; received in revised form 1 February 2004; accepted 8 February 2004
Available online 4 June 2004

Abstract

The tensile and fiber/matrix interfacial properties of 2D and 3D carbon/carbon composites (C/C) were compared. To elucidate the effect of three-dimensional reinforcement, both C/Cs were composed of the same constituents and prepared via. the same process route. The tensile fracture strain of both C/Cs degraded with increasing bulk density, and the fracture strain of the 3D-C/Cs were larger than that of the 2D-C/Cs at the same bulk density. The interfacial bonding strength of the 3D-C/Cs were found to be much lower than that of the 2D-C/Cs. From the comparison of the interfacial and tensile fracture behavior, high tensile fracture strains of 3D-C/Cs were concluded to be attributed to the weak interfacial bonding. This low interfacial strength of the 3D-C/Cs was suggested to be caused by the residual stresses induced during processing in the 3D-C/Cs due to three-dimensional restriction of the fibers.

Keywords: C/C composites; Strength; Interfaces; HIP; Residual stresses

1. Introduction

Carbon/carbon composites (C/Cs) are the only low-density materials that maintain a high strength and toughness at high temperatures up to 3000 °C. Because of this unique advantage, C/Cs have been expected to be used in various high temperature structures especially in the aerospace field.[1–5] However, the mechanical properties of C/Cs have not been sufficiently clarified yet, for example, the ruling mechanism for the basic tensile strength. Thus, the material design of C/Cs has been made relying on experience bases.

Within the last decade, the mechanical properties and fracture behaviors of two-dimensional fiber-reinforced C/Cs (2D-C/Cs) have been widely examined.[6–14] The common results obtained by these studies are; the tensile modulus increases and fracture strain decreases with increasing the final heat treatment temperature (HTT) up to 2500 °C, and the tensile strength and modulus increases with increasing the bulk density. These conclusions were seemed to be drawn only from experimental evidences without any clear understanding of fracture mechanics.

Recently, the present authors and several researchers revealed the ruling mechanisms for achieving high tensile strength of cross-ply laminate C/Cs made of various process routes.[15–17] As a conclusion, the dominant factor for the tensile fracture strains of C/Cs was the bonding strength of the fiber/matrix interface. In other words, the tensile strains to failure systematically increased with weakening the interfacial bonding strength. This tendency is similar to those observed for continuous fiber-reinforced ceramic composites (CFCCs).[18,19] However, this result contains some contradiction with common conclusions mentioned above. For example in our study, the tensile strength of C/Cs degraded with increasing the density. This tendency was caused by the improvement of interfacial bonding with increase in density.

In order to construct a general theory for achieving high tensile strength, the present authors are examining

* Corresponding author. Tel.: +81-42-759-8293; fax: +81-42-759-8461.
E-mail address: hatta@pub.isas.jaxa.jp (H. Hatta).

0955-2219/$ – see front matter © 2004 Elsevier Ltd. All rights reserved.
doi:10.1016/j.jeurceramsoc.2004.02.014

a wide spectrum of C/Cs. The present study about three-dimensionally fiber-reinforced C/Cs (3D-C/Cs) has done within this framework study. One of the characteristics of laminate (2D-) C/Cs is poor interlaminar shear strength (5–20 MPa) that comes from lack of reinforcement in the thickness direction. Thus, 2D-C/Cs can be applied to the structures that sustain only in-plane stress field. To overcome this deficit, 3D-C/Cs are often introduced. However, the mechanism for tensile fracture have been understood little even for 2D-C/Cs and essentially nothing for 3D-C/Cs.

The main purpose of this study is to manifest mechanisms responsible to strengthen 3D-C/Cs and the difference of the fracture modes between 2D- and the 3D-C/Cs. The fracture behavior of 2D- and 3D-C/Cs fabricated through a same process route and composed of same raw materials are examined under tension. The fiber/matrix interface properties were also roughly estimated and the role of the interface on the tensile fracture was discussed.

2. Experimental procedure

2.1. Materials

Mechanical properties of 2D- and 3D-C/Cs fabricated through the same processing route were compared in this study. The precursor for the 2D-C/C was a carbon-fiber-reinforced phenolic resin panel (200 mm × 200 mm × 2 mm) with cross-ply lamination, and the fiber volume fraction of the panel was 60%. In contrast, the precursor for the 3D-C/Cs was 3D-fabric reinforced in orthogonal three *x*, *y*, and *z* directions, where the fiber volume fraction in *x*, *y*, and *z* directions were set to 40, 13, and 3%, respectively. The reinforcing fiber used in both C/Cs was high strength type carbon fiber (Besfite®, IM-600, Toho Rayon Corp., Japan).

After carbonization of resin, carbon matrices were further infiltrated by repeating the hot-isostatic-pressure (HIP) process, in which three steps were repeated: (i) infiltration of coal tar pitch in vacuum; (ii) carbonization at 650 °C at 100 MPa; and (iii) graphitization at 2300 °C in an inert atmosphere. The density of the C/Cs was varied with repetition of the densification cycles. Hereafter, the C/Cs with different bulk density are designated as 3D-C/C-*n* and 2D-C/C-*m*, where *n* and *m* represent the number of the densification cycles applied. The observation of the microstructures of the C/Cs was conducted using a polarized optical microscope (Olympus BH2-UMA, Olympus Optical Co., LTD, Japan).

In addition to above C/Cs, unidirectionally reinforced (UD-) and cross-ply-laminated C/Cs were supplementarily used only for establishing testing methods of the fiber/matrix interfacial-properties. Details of these materials were given in our previous works[6,15] and summarized in Table 1. These supplemental materials will be designated with underline.

2.2. Mechanical testing

2.2.1. Tensile test

Strip shape specimens, length 200 mm and width 10 mm, were used for tensile tests, where the axis of the maximum volume fraction, *x*-axis, was aligned parallel to the loading direction. The tensile specimens were machined into the final shape using a conventional milling technique. The specimen thickness of the 3D-C/Cs was reduced by polishing up to 1.0 mm, where three unit cells were included in the thickness direction. In contrast, thickness of the 2D-C/C specimens was not machined (≈2.0 mm). Tensile tests were carried out using a screw driven testing machine (AG-5000A, Shimadzu Corp., Japan) at a constant cross-head speed of 0.1 mm/min in an ambient air. During the tests, the strain was monitored using two strain gages (effective gage area = 5 mm × 2 mm) affixed on the both sides of a tensile specimen. Since bonding of the strain gages with the C/Cs was weak especially in the case of low density 3D-C/C due to porous nature, epoxy resin was thinly coated under strain gages (Fig. 1).

2.2.2. Interfacial strength tests

The interfacial strength of the C/Cs was evaluated using a fiber-bundle push-out (FBP) method illustrated in Fig. 3.[21] In this method, the interfacial fracture was induced by a load applied with a cylindrical indenter to a layer or fiber bundle, in which the fibers placed parallel to the loading direction as shown in Fig. 3(b) and (c). Since the layer thickness of the 2D-C/Cs was about 125 μm and bundle thickness of 3D-C/Cs was 200–300 μm, the indenter diameter was set to 50 μm for these C/Cs. The base plate possessed a groove, which enabled a cylindrical C/C rod to be pushed out. Specimen thickness of 2D- and 3D-C/Cs were arranged to approximately 200 μm except for the discussion on dimensional effect, and the load was applied using a screw-driven

Table 1
Materials and their specification

Materials	Fiber (V_f %)	Fabrication process	HTT (°C)	ρ (kg/m^3)	References[a]
2D-C/C	IM600 (60)	HIP	2300	1600–2000	–
3D-C/C	IM600 (56)	HIP	2300	1600–2000	–
UD – C/C	M 46J (50)	Preformed yarn	2000	1750	6,11
2D – C/C	IM600 (60)	Resin char	2300	1300–1800	15,20

[a] Detailed processing routes and conditions were given.

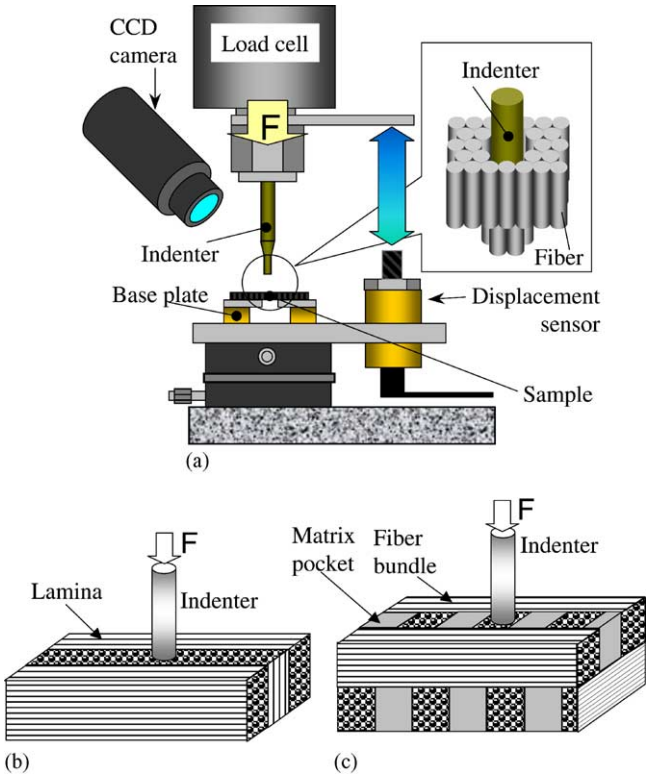

Fig. 1. Schematic drawings of fiber bundle push-out test: (a) 2D-C/C specimen; (b) and 3D-C/C specimen; (c) used in FBP tests.

mechanical testing machine (Orientec RTM-25, maximum load; 25 kgf) under a crosshead speed of 0.1 mm/min.

2.2.3. Tensile strength of carbon fiber

The heat treatment temperature of the carbon fiber IM-600 is supposed to be around 1300–1500 °C.[22] The examined C/Cs in this study were heat-treated at a temperature of 2300 °C. Thus, the tensile strength of the fiber would be expected to differ from that given in the supplier's data. Thus, the distribution of fiber tensile strength after heat treatment at 2300 °C was measured using a method specified in Japanese Standard JIS R 7606. In this Japanese standard, a single fiber with a length of 55 mm is fixed to a paper holder, in which the gage length is set to 25 mm. Tensile tests for this study were performed under a crosshead speed of 1.0 mm/min using a screw-driven tensile testing machine, Orientec RTM-25. At least 30 tests were performed for determination of average strength of the heat-treated carbon fibers.

3. Experimental results

3.1. Preliminary results

3.1.1. Micro-structure and pore size distribution

Fig. 2 shows the variation of the bulk density with HIP cycles for the 2D- and the 3D-C/Cs. The 3D-C/Cs possessed lower bulk density than the 2D-C/Cs at the same number of process cycles until three cycles, and they became nearly the same from four cycles. The cross-sections of the C/Cs were observed to elucidate the differences of the micro-structure. Fig. 3(a) and (b) show the micro-photos of 3D-C/C-2 and

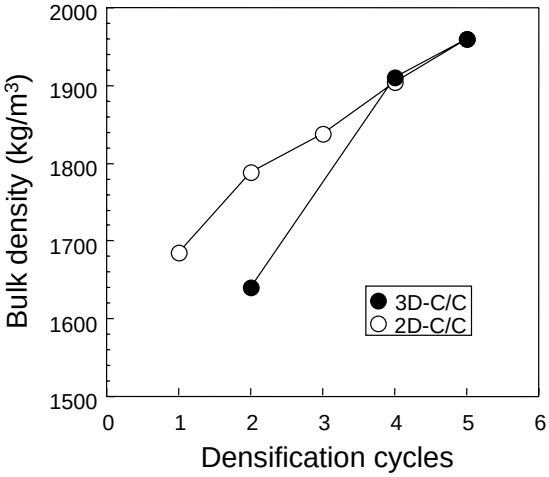

Fig. 2. Bulk density of the C/Cs as a function of densification cycles.

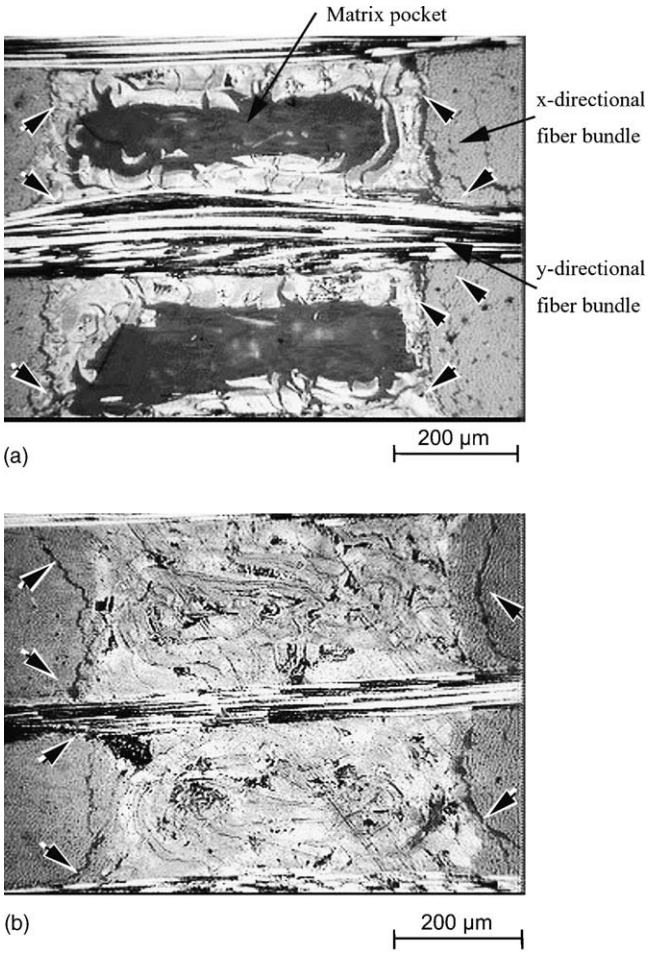

Fig. 3. Micro-photos around matrix pocket in the 3D-C/Cs: (a) 3D-C/C-2 and (b) 3D-C/C-5. Small arrows indicate the cracks running along the fiber bundles.

3D-C/C-5, respectively. In three-dimensionally orthogonal fabrics, large vacant spaces are formed and usually referred to as matrix pockets. It can be seen in these photos that the pockets were gradually filled with matrix carbon by the repetition of HIP cycles, and the matrix pockets were almost fully infiltrated at the 5th cycle. Voids in fiber bundles were also filled with the infiltration process. The defects along the fiber/matrix interface should also be filled by matrix carbon, though it is not observed due to low magnification images. On the other hand, a typical defect appearing in the 2D-C/C was so called transverse cracks,[15,23] which extend through-the-ply and run parallel to the fiber axis.

3.1.2. Fiber bundle push-out (FBP) test

A typical load-displacement curve obtained by the FBP test is shown by a solid line in Fig. 4. In FBP tests, complete debonding on the fiber/matrix interfaces occurred at a maximum load F_{max}, and the interfacial sliding proceeded from a load of F_s. Thus, the debonding shear stress τ_d and sliding stress t_s were approximately determined by the loads, F_{max}, and F_s divided by the area of the fracture surface. The dotted line in Fig. 4 is a typical load-displace curve when fibers in the bundle fractured in compressive mode (photo in Fig. 4). In such a case, double or triple peaks were observed around the F_{max}, and the steep load drop from the F_{max} to F_s was not observed. A hole in a UD-C/C specimen produced by a FBP test and a pushed-out fiber bundle were shown in Fig. 5(a) and (b), respectively. As these photos show, FBP specimens predominantly fractured along fiber/matrix interfaces. However, small chipping of fibers was observed near the loading edge as indicated by white arrows. Since the chipping occurred due to location mismatch between the indenter edge and fiber interfaces, this phenomenon was observed most of FBP tests. However, because chipping size was small compared with the rest of fracture area, the FBP test was judged to be effective to measure interfacial bonding (Fig. 5).

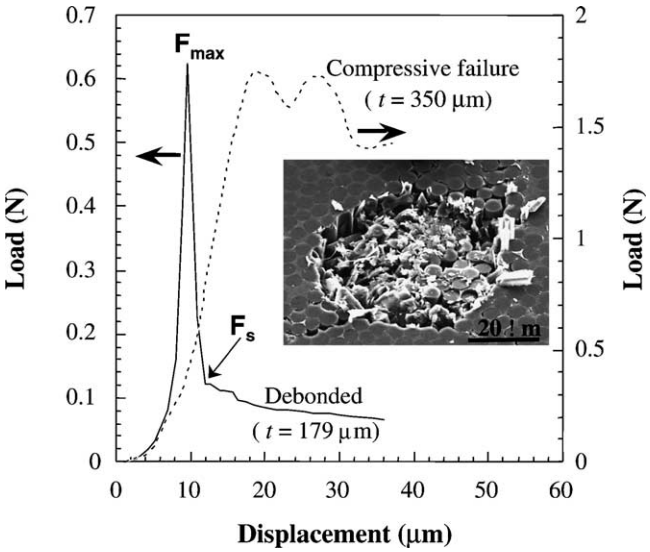

Fig. 4. Typical load-displacement curves of UD-C/C obtained by the fiber bundle push-out tests when fracture occurred along interface (solid line) and fibers fractured by compressive load (dotted line and photo in figure).

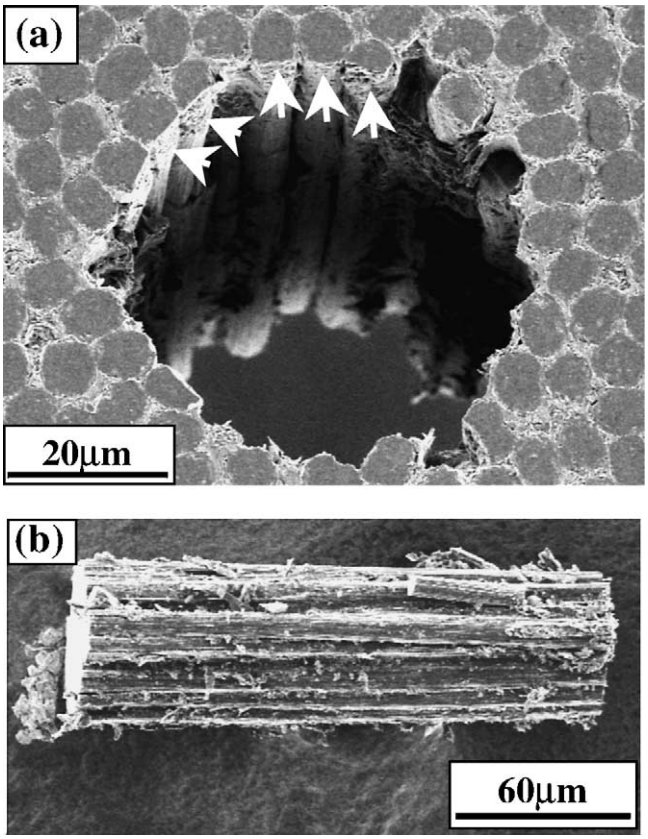

Fig. 5. Scanning electron micro-photographs of the UD-C/C specimen after fiber bundle push-out tests ($D = 50\,\mu m$). The arrows indicate chopped fibers by the edge of plunger. This type of damage was observed only near the surface: (a) top surface near the pushed-out hole and (b) completely pushed-out fiber bundle.

The advantage of the FBP method is easy to perform compared with a single fiber push-out, SFP, test. The SFP tests were also conducted using a micro-Vickers indenter. However, thin specimens appropriate for the SFP tests were extremely difficult to prepare, for example, when a specimen had weak interface, and in many cases resulted in compressive failure of the fiber.[21] The interfacial debonding stresses obtained by the FBP and SFP tests were compared in Fig. 6. As this figure shows, although absolute values by the FBP and SFP tests differ, tendencies are similar, and the difference might be a size effect (indenter diameter: 50 μm, fiber diameter: 5 μm) possibly explained using the concept of the fracture mechanics. Thus, the FBP test was adopted in this study for the evaluations of interfacial debonding and sliding stresses.

3.2. Comparison of 2D- and 3D-C/Cs

3.2.1. Tensile strength

Fig. 7 shows the stress–strain (σ–ε) relations of the 3D-C/Cs obtained by tensile tests. The strain measurements

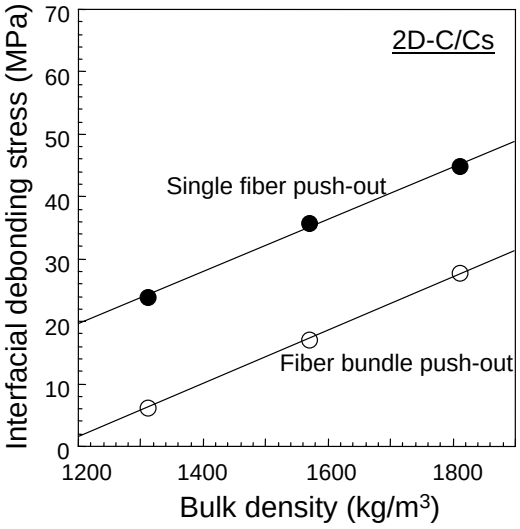

Fig. 6. Comparison of the interfacial debonding stress obtained by the single fiber push-out and the fiber bundle push-out tests.

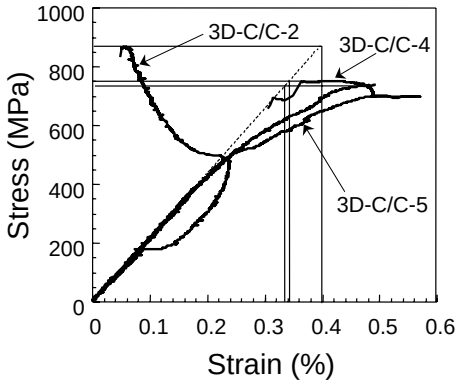

Fig. 7. Tensile stress–strain curves of the 3D-C/Cs. Dotted line indicates the estimation scheme of the fracture strain.

by strain gages failed from applied strains, 3D-C/C-2 ≈ 0.08%, 3D-C/C-4 ≈ 0.25%, and 3D-C/C-5 ≈ 0.45%. These gage failures were caused by the premature fracture occurred near the surfaces of the specimens, as shown in Fig. 8. In the 3D-C/Cs, the initial fracture always located on the surface. This was supposed to be caused by low shear strength[23,24] due to low interfacial bonding between the fiber and matrix. When shear strength is extremely low, only a part of load is transferred to inner specimen, because the tensile load transfers from a test fixture to specimen by shear stress. Thus, surface regions adhered to tub sustained a larger stress than inner region. This tendency became distinguishing when density of C/Cs lowered, because shear strength decrease with lowering the density.[24] It follows from above discussion that the 3D-C/Cs can sustain more load if the shear strength is higher.

The tensile strength of the 3D-C/Cs in Fig. 7 exhibited the maximum value of 870 MPa for 3D-C/C-2 and degraded with repetition of the infiltration cycles, 760 MPa for 3D-C/C-4 and 750 MPa for 3D-C/C. The fracture strain was estimated by assuming that modulus was not changed during the tensile testing as shown by straight dotted lines in Fig. 7. The fracture strains thus evaluated are 0.39, 0.34, and 0.33 for 3D-C/C-2, -4, and -5, respectively. The initial

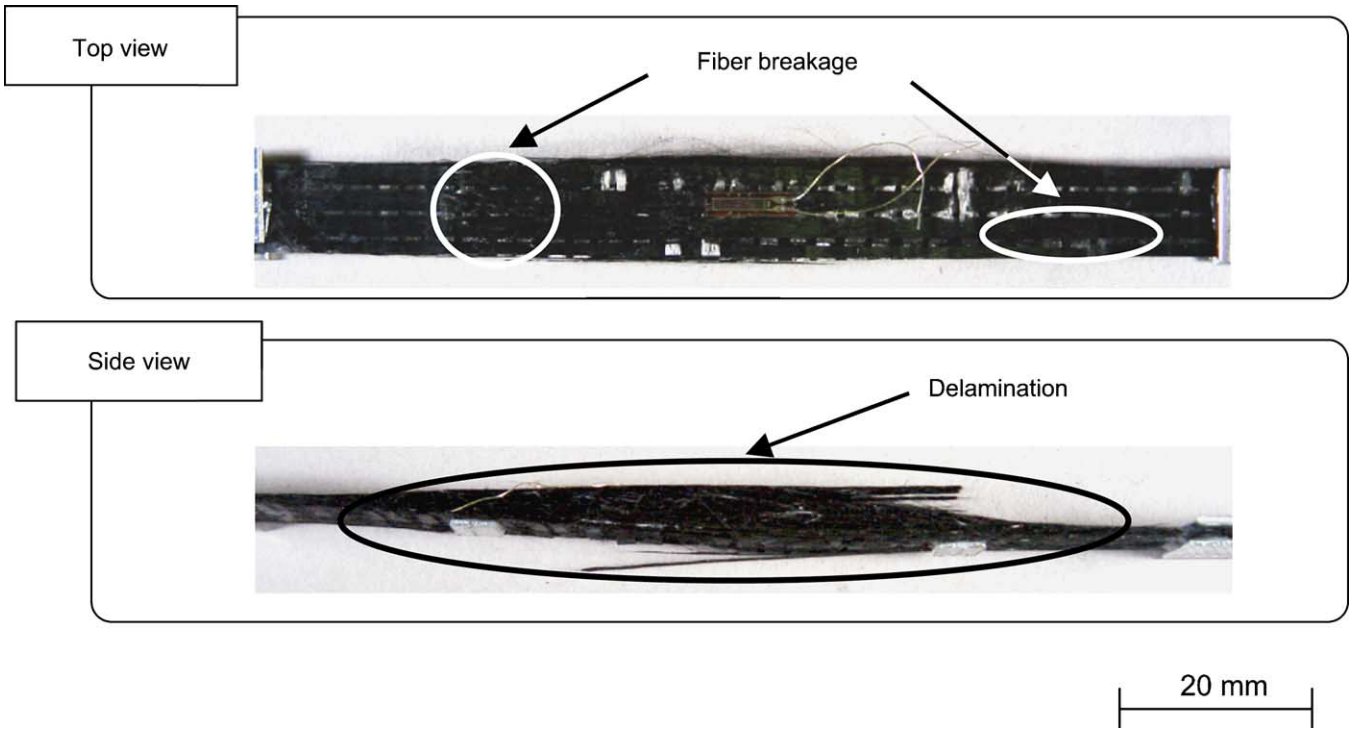

Fig. 8. Fracture pattern of the 3D-C/C-2.

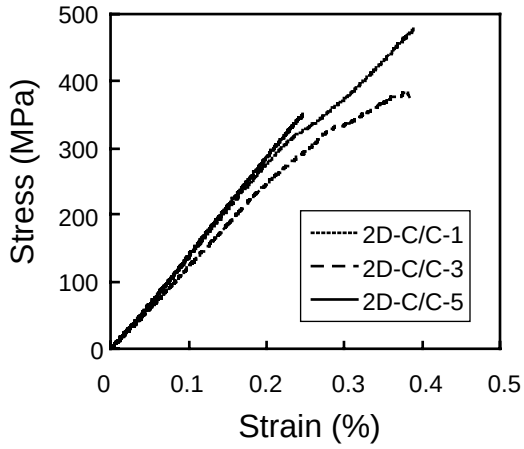

Fig. 9. Stress–strain curves of the 2D-C/Cs obtained by tensile tests.

tensile modulus increased with the infiltration cycles from 195 GPa (3D-C/C-2) to 215 GPa (3D-C/C-5). These tendencies of the mechanical properties were identical to those of the 2D-C/Cs as shown in Fig. 9. For the 2D-C/Cs, the σ–ε relation became nonlinear with slight modulus degradation from the strain level of 0.25%. Comparison was made of the fracture strains of the 3D-C/Cs with those of the 2D-C/Cs in Fig. 10. Note that tensile fracture strains of the 3D-C/Cs are higher than those of the 2D-C/Cs, even though the linear σ–ε curved assumed only for the 3D-C/Cs.

The observation of the fracture appearances of the C/Cs revealed variation in fracture patterns. As shown in Fig. 8, the 3D-C/C-2 shows a broom-like fracture with fiber-bundle unit debonding throughout the specimen. This fact suggested low bonding strength between fiber/matrix interface. On the contrary, such intensive debonding was not observed in the 3D-C/C-5. The fracture surface of the 2D-C/Cs with low density and high strength was more serrated and the fractured area spread out. The serration in the 2D-C/C-1s or -2 was

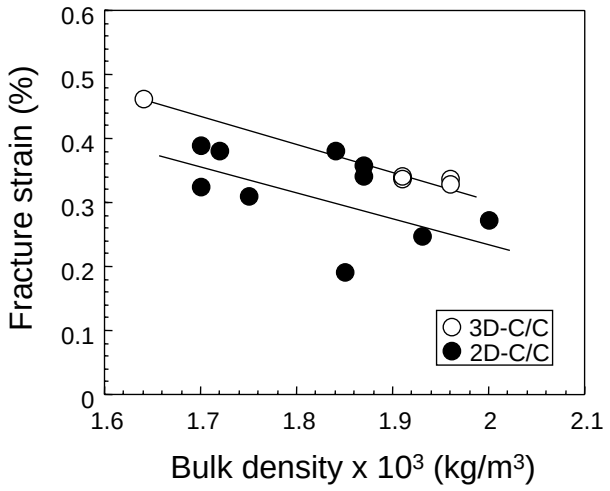

Fig. 10. Fracture strains of the 2D- and the 3D-C/Cs as a function of bulk density.

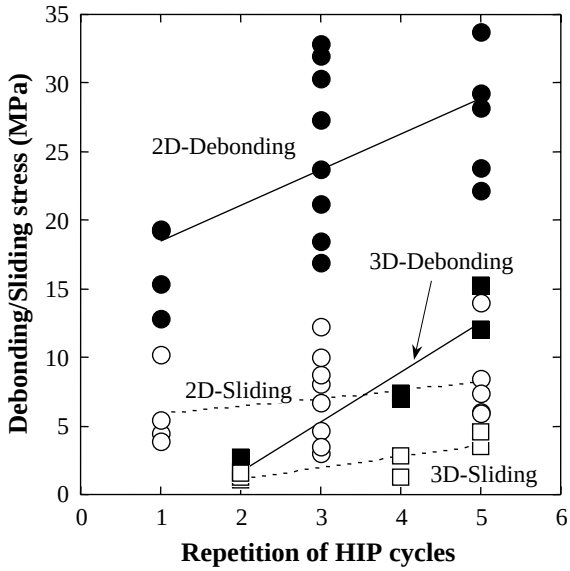

Fig. 11. The interfacial debonding and sliding stresses between the fiber and matrix of 2D- and 3D-C/Cs as functions of HIP cycles.

in the fiber unit, but that in the 3D-C/C-2s was in the fiber bundle unit. In contrast, the 2D-C/C-5s near straight fracture surface without debonding of fiber interface.[15]

3.2.2. Interfacial bonding

Tensile fracture strain and fracture patterns of C/Cs have suggested to be characterized by the interfacial bonding strength between the fiber and matrix.[15] Hence, an attempt was made to determine the interfacial debonding and sliding stresses of these C/Cs. In Fig. 11, the interfacial debonding and sliding stresses of the 2D- and 3D-C/Cs are shown as a function of repetition of HIP cycles. It is noted in these results that the interface of the 3D-C/Cs are much weaker than that of the 2D-C/Cs. In addition, the interfacial debonding and sliding stresses of the 2D- and 3D-C/Cs are increased with increasing the bulk density.

3.2.3. Fiber strength

During microscopic observations of the C/Cs, we notice diametric change of the carbon fibers, as shown in Fig. 12. The data at the 0 HIP cycle in this figure represents diameter of the IM-600 fiber in the resin charred 2D-C/C heat-treated at 2573 K without (the as received fiber (without heat-treatment) had a diameter of 5.35 μm). This figure shows that the fiber diameter gradually shrank during repetitive HIP treatments. This reduction in the fiber diameter might give rise to fiber strength degradation. For example, heat treatment without mechanical constraint also led to fiber radius reduction with increasing heat treatment temperature.[25] The tensile strength IM600 fiber in that situation was found to linearly lower with decreasing fiber radius, as shown in Fig. 13. After five cycles of the HIP treatment, the average diameter of the fiber was lowered from 4.9 to 4.7 μm. This reduction might induce degradation of fiber

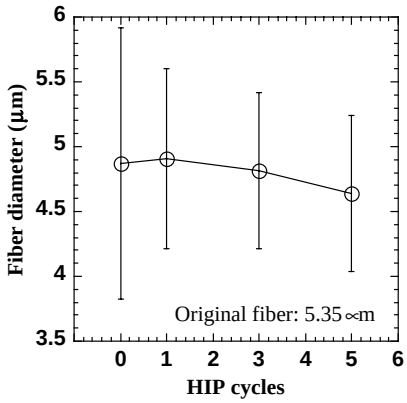

Fig. 12. Variation of fiber diameter in the C/Cs with repetition of HIP cycles.

strength; using Fig. 12 the degradation can be estimated from 4.5 to 3.35 GPa. This result indicates that fiber strength degradation should be taken into account in the present study.

3.2.4. Tensile strength

The above results suggest that principal parameters having serious influence on the tensile strength of the C/Cs are interfacial bonding strength and fiber strength. Hence, the tensile fracture strains are plotted in Fig. 14 as functions of the interfacial debonding stress, where the data are set into groups by the number of HIP cycles, because of the fiber degradation. For comparison purpose, the fracture strains of 2D-C/Cs fabricated by resin-char method (reinforced by the same fiber, IM600, and treated by the same HTT, 2300 °C)[20] are also plotted in this figure. It follows from this figure that the strengths of the HIPed C/Cs decrease with increasing interfacial strength, and the decrease rate is nearly the same as the resin-charred C/Cs.

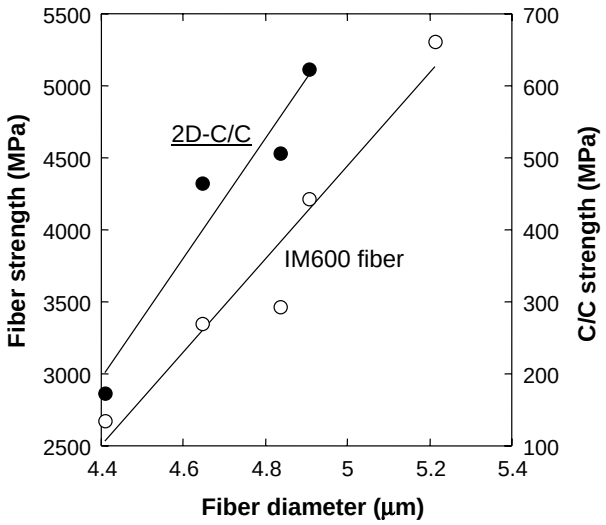

Fig. 13. Strength of IM600 fiber and C/C reinforced with IM600 fiber, processed by resin char method, and heat-treated at 2300 °C as a functions of. fiber diameter.

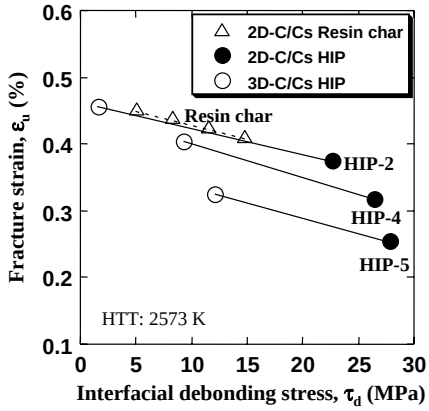

Fig. 14. Tensile fracture strains of HIPed 2D- and 3D-C/Cs compared with those of resin-charred 2D-C/Cs.

4. Discussion

4.1. Residual stresses in the 2D- and 3D-C/Cs

One of dominant properties controlling the difference of tensile strength of the 2D- and 3D-C/Cs were shown to be the difference in the interfacial bonding. As the source yielding the difference in the interface bonding, let us discuss residual stresses in C/Cs. Residual stresses in C/Cs are mainly induced by the following two mechanisms:

(1) Mismatch in thermal expansion in the fiber axis and transverse directions, which appears during cooling stage after heat treatment.
(2) Shrinkage of the matrix during the carbonization and graphitization stages.

These mechanisms yield the same type of residual stresses. When cross-sections shown in Fig. 15 are considered, it can be seen that the residual stress induced in the 2D-C/Cs is essentially uni-axial tension in the ply-interfacial direction, and that in the 3D-C/Cs is bi-axial tension. Because of these tensile stresses, transverse cracks are generated parallel to the fiber axes in the 2D-C/Cs, as illustrated in

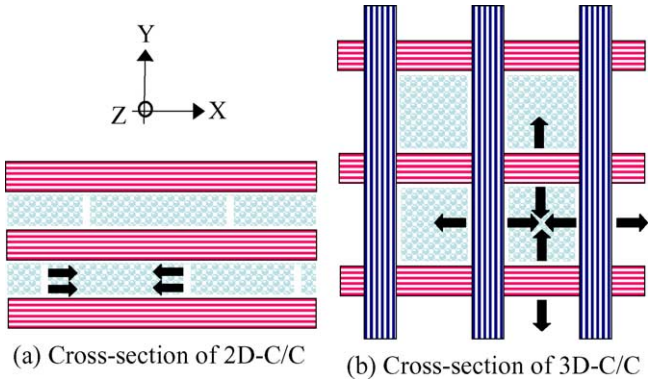

Fig. 15. Schematic drawing illustrating thermal stresses induced in the 2D-C/Cs and the 3D-C/Cs.

Fig. 15(a), whereas inter-and intra-bundles cracks were induced in the 3D-C/Cs. It was already verified that due to three-dimensional constraints, thermal residual stresses in 3D composites are much higher than those in the 2D composites.[26,27] Thus, in the 3D-C/Cs, the cracks should be much larger and of higher density than in the 2D-C/Cs, and interfacial strength of the 3D-C/Cs must become much weaker than that of the 2D-C/Cs.

5. Conclusions

The fracture behaviors of the 2D- and 3D-C/Cs processed via the same matrix densification route and possessing the same raw materials were compared, and the following conclusions are obtained.

(1) The tensile strength of the 3D-C/Cs was much lower than that of the 2D-C/Cs.
(2) The interfacial bonding of the 3D-C/Cs was much weaker than that of the 2D-C/Cs at the same bulk density.
(3) Fracture strain of the 2D- and 3D-C/Cs can be characterized by interfacial bonding strength and fiber strength.

Acknowledgements

This study was financially supported in part by a grant-in-aid for basic science (grant no. 11305047) from the Ministry of Education, Science, Sports and Culture, Japan.

References

1. Fitzer, E., The future of carbon–carbon composites. *Carbon* 1987, **25**(2), 163–190.
2. Buckley, J. D., *Carbon–Carbon Materials and Composite*. NASA Reference Publication, 1992, p. 1254.
3. Schmidt, D. L., Davidson, K. E. and Theibert, L. S., Unique applications of carbon–carbon composite materials (part one). *SAMPE J.* 1999, **35**(3), 27–39.
4. Schmidt, D. L., Davidson, K. E. and Theibert, L. S., Unique applications of carbon–carbon composite materials (part two). *SAMPE J.* 1999, **35**(4), 51–63.
5. Schmidt, D. L., Davidson, K. E. and Theibert, L. S., Unique applications of carbon–carbon composite materials (part three). *SAMPE J.* 1999, **35**(5), 47–55.
6. Kogo, Y., Hatta, H., Kawada, H. and Machida, T., Effect of stress concentration on tensile fracture behavior of carbon–carbon composites. *J. Comp. Mater.* 1998, **32**(13), 1273–1294.
7. Brondsted, P., Heredia, F. E. and Evans, A. G., In-plane shear properties of 2-D ceramic matrix composite. *J. Am. Ceram. Soc.* 1994, **77**(10), 2569–2574.
8. Turner, K. R., Speck, J. S. and Evans, A. G., Mechanisms of deformation and failure in carbon–matrix composites subject to tensile and shear loading. *J. Am. Ceram. Soc.* 1995, **78**(7), 1841–1848.
9. Namiki, F. and Chou, T. W., Tensile behavior of a quasi-isotropic carbon–carbon composite. *J. Am. Ceram. Soc.* 1998, **81**(1), 113–120.
10. Thielicke, B., Mechanical properties of C/C composites. *Key Eng. Mater.* 1999, **164/165**, 145–150.
11. Hatta, H., Kogo, Y., Asano, T. and Sawada, Y., Pin joint strength of C/C composites. *J. Jpn. Soc. Mech. Eng. A* 1997, **63**(611), 1586–1593.
12. Kogo, Y., Hatta, H., Toyoda, M., Goto, K. and Sugibayashi, T., Strength and fracture behavior of dovetail joint structure made of 2D carbon–carbon composite. *J. Jpn. Soc. Comp. Mater.* 1998, **24**(6), 222–229 [in Japanese].
13. Heredia, F. E., Spearing, S. M., Evans, A. G., Mosher, P. and Curtin, W. A., Mechanical properties of continuous-fiber-reinforced carbon matrix composite and relationship to constituent properties. *J. Am. Ceram. Soc.* 1992, **75**(11), 3017–3025.
14. Siron, O. and Lamon, J., Damage and failure mechansms of a 3-dimensional carbon/carbon composite under uniaxial tensile and shear loads. *Acta Mater.* 1998, **46**(18), 6631–6643.
15. Hatta, H., Suzuki, K., Shigei, T., Somiya, S. and Sawada, Y., Strength improvement by densification of carbon–carbon composite. *Carbon* 2001, **39**, 83–90.
16. Trouvat, B., Bourrat, X. and Naslain, R., *Toughening Mechanism in C/C Minicomposites with Interface Control, Extended Abstracts and Program of Carbon '97 Vol II*. The American Carbon Society, 18–23 July, 1997, pp. 536–537.
17. Hayashi, M., Niijima, K. and Saito, K., Studies on high strength C/C composites with PAN-based carbon fiber. In *Proceedings of 2nd Japan International SAMPE Symposium*. 1991, pp. 889–896.
18. Evans, A. G. and Zok, F. W., Review: the physics and mechanics of fibre-reinforced brittle matrix composites. *J. Mater. Sci.* 1994, **29**, 3857–3896.
19. Thouless, M. D., Sbaizero, O., Sigl, L. S. and Evans, A. G., Effect of interface mechanical properties on pullout in a SiC-fiber-reinforced lithium aluminum silicate glass-ceramic. *J. Am. Ceram. Soc.* 1989, **72**(4), 525–532.
20. Hatta, H., Aoi, T., Kawahara, I. and Kogo, Y., Tensile strength of carbon/carbon composites II: Effect of heat treatment temperature for C/C reinforced with PAN-based fiber. *J. Compos. Mater.*, in press
21. Furukawa, Y., Hatta, H. and Kogo, Y., Interfacial shear strength of C/C composites. *Carbon* 2003, **41**, 1819–1826.
22. Fitzer, E. and Manocha, L. M., *Carbon Reinforcements and Carbon/Carbon Composites*. Springer-Verlag, New York, 1998.
23. Aly-Hassan, M. S., Hatta, H., Wakayama, S., Watanabe, M. and Miyagawa, K., Comparison of 2D and 3D carbon/carbon composites with respect to damage and fracture resistance. *Carbon* 2003, **41**, 1069–1078.
24. Denk, L., Hatta, H., Misawa, A. and Somiya, S., Shear fracture of C/C composites with variable stacking sequence. *Carbon* 2001, **39**(10), 1505–1513.
25. Hatta, H., Aoi, T., Kawahara, I., Kogo, Y. and Shiota, I., Tensile strength of carbon/carbon composites I: Effect of density and interfacial strength. *J. Compos. Mater.*, in press.
26. Hatta, H., Takei, T. and Morii, A., Thermo-mechanical properties of resin matrix 3D fabric composites. *Mater. Syst.* 1991, **10**, 71–80 [in Japanese].
27. Hatta, H., Takei, T. and Taya, M., Effect of dispersed microvoids on thermal expansion behavior of composite materials. *Mater. Sci. Eng. A* 2000, **A285**, 99–110.